Strong Constraints to the Putative Planet Candidate around VB 10 using Doppler spectroscopy [1]

Guillem Anglada-Escudé

Department of Terrestrial Magnetism, Carnegie Institution of Washington
5241 Broad Branch Road, NW, Washington, DC 20015 USA

anglada@dtm.ciw.edu

Evgenya Shkolnik

Department of Terrestrial Magnetism, Carnegie Institution of Washington
5241 Broad Branch Road, NW, Washington, DC 20015 USA

shkolnik@dtm.ciw.edu

Alycia J. Weinberger

Department of Terrestrial Magnetism, Carnegie Institution of Washington
5241 Broad Branch Road, NW, Washington, DC 20015 USA

weinberger@dtm.ciw.edu

Ian B. Thompson

The Observatories of the Carnegie Institution of Washington
813 Santa Barbara Street, Pasadena, CA 91101 USA

ian@obs.carnegiescience.edu

David J. Osip

Las Campanas Observatory, Carnegie Institution of Washington
Colina El Pino Casilla 601, La Serena, Chile

dosip@lco.cl

John H. Debes

Goddard Space Flight Center, NASA Postdoctoral Program
8463 Greenbelt Rd, Greenbelt, MD 20770, USA

john.H.debes@nasa.gov

ABSTRACT

We present new radial velocity measurements of the ultra-cool dwarf VB 10, which was recently announced to host a giant planet detected with astrometry. The new observations were obtained using optical spectrographs(MIKE/Magellan and ESPaDOnS/CHFT) and cover a 63% of the reported period of 270 days. We apply Least-squares periodograms to identify the most significant signals and evaluate their corresponding False Alarm Probabilities. We show that this method is the proper generalization to astrometric data because (1) it mitigates the coupling of the orbital parameters with the parallax and proper motion, and (2) it permits a direct generalization to include non-linear Keplerian parameters in a combined fit to astrometry and radial velocity data. In fact, our analysis of the astrometry alone uncovers the reported 270 d period and an even stronger signal at ∼50 days. We estimate the uncertainties in the parameters using a Markov Chain Monte Carlo approach. The nominal precision of the new Doppler measurements is about 150 s^{-1} while their standard deviation is 250 ms^{-1}. However, the best fit solutions still have RMS of 200 ms^{-1} indicating that the excess in variability is due to uncontrolled systematic errors rather than the candidate companions detected in the astrometry. Although the new data alone cannot rule-out the presence of a candidate, when combined with published radial velocity measurements, the False Alarm Probabilities of the best solutions grow to unacceptable levels strongly suggesting that the observed astrometric wobble is not due to an unseen companion.

Subject headings: astrometry, methods: statistical, stars: individual (VB 10), techniques: radial velocities

1. Introduction

Pravdo & Shaklan (2009) recently announced the discovery of an astrometric companion to VB 10, an ultra-cool dwarf with a mass of ≈0.08 $M_\odot$. From a Keplerian fit to the motion, they determined a mass of 6 M_J and a period of 270 d. Thus VB 10 became the lowest mass star known to harbor a planetary companion. The mass ratio between VB 10 and its companion, ∼13, also is intriguing. A similar mass ratio for a Solar-type star would make the companion a brown dwarf, but brown dwarfs as small separation companions to stars are quite rare. VB 10 is itself the secondary in a wide binary with V1428 Aql, a M2.5 star (van Biesbroeck 1961). At a distance of

[1]Based on observations collected with the 6.5 meter Magellan Telescopes located at Las Campanas Observatory, Chile, at the W. M. Keck Observatory and the Canada-France-Hawaii Telescope (CFHT). The Keck Observatory is operated as a scientific partnership between the California Institute of Technology, the University of California, and NASA, and was made possible by the generous financial support of the W. M. Keck Foundation. CFHT is operated by the National Research Council of Canada, the Institut National des Sciences de l'Univers of the Centre National de la Recherche Scientique of France, and the University of Hawaii.

5.8 pc from the Sun, the 74″ separation of this proper motion binary corresponds to a projected separation of 430 AU.

Such low-mass stars have not been the target of intensive precision radial velocity (PRV) monitoring because they have low visual fluxes and high stellar activity. For example, the dedicated HARPS M-dwarf planet search observes stars[2] only brighter than V=14 and of moderate to low activity levels (Bonfils et al. 2007). VB 10 has V mag = 17.3 and is known to be a flare star (Berger et al. 2008). PRV and lensing planet searches have so far found only 13 stars under 0.5 $M_\odot$ hosting 18 planets, and of these, more than half have masses below 0.1 M_J.

Despite the challenges, searches for planetary companions to low mass stars are of continuing interest. Low-mass stars appear less likely to have lower mass stellar companions and less likely to harbor planets than Solar-mass stars (Cumming et al. 2008). When they do have companions, they tend to be stars of nearly equal mass to the primary (Burgasser et al. 2007). The mass function of planets orbiting M dwarfs, and how it differs from the planet mass function for higher-mass stars, provides a constraint on the planet formation mechanism(s) in general. Disks sufficiently massive to form Jupiter-mass planets appear to be rare around brown dwarfs, whose disks generally look like lower mass versions of T Tauri disks (Scholz et al. 2006). High mass companions would have to form via a binary-like fragmentation mechanism (e.g. Font-Ribera et al. 2009). Thus how a 6 M_J planet could form around an ∼80 M_J star and how common such high-mass ratio companions remain important questions (Boss et al. 2009).

The reported planet's astrometric orbit predicts a radial velocity (RV) amplitude of at least 1 km s^{-1} for a circular orbit and up to several km s^{-1} for an eccentric orbit. This magnitude signal is detectable with ordinary RV measurements without requiring the adoption of precision techniques such as an iodine cell or simultaneous thorium reference.

Although several RV measurements of VB 10 exist in the literature before 2009, it is difficult to combine the historical RVs (see list in Table 4 of Pravdo & Shaklan (2009)), as each observation used different calibration techniques and/or RV standards that introduce zero-point offsets and the typical uncertainties are also large (∼1.5 km s^{-1}). The most precise measurements in the literature were recently published by Zapatero Osorio et al. (2009) (hereafter Z09), but provide only a "hint of variability." These data did little to constrain the orbital parameters of the planet beyond what the astrometry had already done (Anglada-Escudé et al. 2009).

Here, we present a more precise set of RV observations over 175 days (or 65% of the reported orbital period). We also present general techniques for joint fitting of astrometric and RV data and show how they can be used to constrain the orbit of the candidate planet.

[2]http://www.eso.org/sci/observing/proposals/77/gto/harps/3.txt

2. New Data

We acquired spectra at 7 epochs in 2009 with the MIKE spectrograph at the Magellan Clay telescope at Las Campanas Observatory (Chile). We used the 0.35″ and the 0.5″ slits which produce a spectral resolution of ≈45,000 and 35,000, respectively, across the 4900 – 10000Å range of the red chip. The seeing was in the range from 0.5 to 1.1″. These data were reduced using the facility pipeline (Kelson 2003).

We also have in hand a single spectrum of VB 10 taken in 2006 using the HIRES (Vogt et al. 1994)) on the Keck I 10-m telescope. We used the 0.861″ slit to obtain a spectral resolution of $\lambda/\Delta\lambda$≈58,000 at $\lambda \sim 7000\AA$. We used the GG475 order-blocking filter and the red cross-disperser to maximize throughput in the red orders.

To increase the phase coverage, an additional spectrum was obtained using the ESPaDOnS on the CFHT 3.6-m telescope. ESPaDOnS is fiber fed from the Cassegrain to Coudé focus where the fiber image is projected onto a Bowen-Walraven slicer at the spectrograph entrance. ESPaDOnS' 'star+sky' mode records the full spectrum over 40 grating orders covering 3700 to 10400 Å at a spectral resolution of $\lambda/\Delta\lambda$≈68,000. The data were reduced using *Libre Esprit* described in Donati et al. (1997, 2007).

Each stellar exposure is bias-subtracted and flat-fielded for pixel-to-pixel sensitivity variations. After optimal extraction, the 1-D spectra are wavelength calibrated with a thorium-argon arc. To correct for instrumental drifts, we used the telluric molecular oxygen A band (from 7620 – 7660 Å) which aligns the MIKE spectra to 40 m s^{-1}, after which we corrected for the heliocentric velocity. Consistency tests with the bluer Oxygen band shows comparable values but with larger measurement error.

The final spectra are of moderate S/N reaching ≈ 25 per pixel at 8000 Å. Each night, spectra were also taken of a M-dwarf RV standard, namely GJ 699 (Barnard's star; SpT = M4V) and/or GJ 908 (SpT = M1V).

To measure VB 10's RV, we cross-correlated each of 9 orders between 7000 and 9000 Å (excluding those with strong telluric absorption) where VB 10 emits most of its optical light, with the spectrum of GJ 699 and/or GJ 908 taken on the same night using IRAF's[1] *fxcor* routine (Fitzpatrick 1993). Both GJ 699 and GJ 908 have been monitored for planets for years and none has been found within the RV stability level of 0.1 km s^{-1}. Here we use the systemic RVs published by a planet-search team (Nidever et al. 2002): RV(GJ 699) = –110.506 km s^{-1} and RV(GJ 908) = –71.147 km s^{-1}. The zero-point of the absolute RVs is uncertain at the 0.4 km s^{-1} level. We measured the RVs from the gaussian peak fitted to the cross-correlation function (CCF) of each order and adopt the average RV of all orders with a mean standard deviation of the individual measurements of 0.150 km s^{-1}. The average of all our measurements is 36.02 km s^{-1} with a standard deviation

[1]IRAF (Image Reduction and Analysis Facility), http://iraf.noao.edu/

of 0.25 km s^{-1}. An observing log with the measured RVs and uncertainties for VB 10 is shown in Table 1.

3. Data Analysis: Combining Astrometry and Radial Velocities

In this section, we reanalyze the original astrometric data to calculate the likelihood of astrometrically allowed solutions, and then combine the astrometry and RV data sets in a consistent framework to quantify how the new RV measurements constrain the possible orbits of the candidate signals observed in the astrometry of VB 10b.

3.1. Least-squares periodograms

The most popular method to look for periodicities in data is the so-called Lomb-Scargle periodogram. A version adapted to deal with astrometric two-dimensional data developed by Catanzarite et al. (2006) (Joint Lomb Scargle periodogram) was implemented in the discovery paper of VB 10b (Pravdo & Shaklan 2009). Any method based on the Lomb-Scargle periodogram performs optimally only under an important implicit assumption: all other signals (e.g. linear trend, an average offset, etc.) can be subtracted from the data without affecting the significance of the signal under investigation. This assumption does not hold for astrometry because the proper motion and the parallax are also a significant part of the signal and they typically correlate with the periodic motion of a planet (see Black & Scargle 1982).

We use instead a Least-squares periodogram. The weighted Least-squares solution is obtained by fitting all the free parameters in the model for a given period. The sum of the weighted residuals divided by N is the so-called χ^2 statistic. Then, each χ^2_P of a given model with k_P parameters, can be compared to the χ^2_0 of the null hypothesis with k_0 free parameters by computing the power, z, as

$$z(P) = \frac{(\chi^2_0 - \chi^2_P)/(k_P - k_0)}{\chi^2_P/(N_{\rm obs} - k_P)} \tag{1}$$

where a large z is interpreted as a very significant solution. The values of z follow a Fisher F-distribution with $k_P - k_0$ and $N_{\rm obs} - k_P$ degrees of freedom (Scargle 1982; Cumming 2004). Even if only noise is present, a periodogram will contain several peaks (see Scargle 1982, as an example) whose existence have to be considered in obtaining the probability of a spurious detection. Assuming Gaussian noise, the probability that a peak in the periodogram has a power higher than $z(P)$ by chance is the so-called False Alarm Probability (FAP) :

$$\mathrm{FAP} = 1 - (1 - \mathrm{Prob}[z > z(P)])^M \tag{2}$$

where M is the number of independent frequencies. In the case of uneven sampling, M can be quite large and is roughly the number of periodogram peaks one could expect from a data set with only

Gaussian noise and the same cadence as the real observations. We adopt the recipe $M \approx 2\Delta T/P_{min}$ given in Cumming (2004, Sec 2.2), where ΔT is the time-span of the observations and $P_{\rm min}$ is the minimum period searched. One still has to select $P_{\rm min}$ arbitrarily. Assuming a $P_{\rm min} = 20$ days, the astrometric data alone has $M \sim 300$, and the combination of astrometry and RVs has $M \sim 360$.

In our particular problem, the null hypothesis is the basic kinematic model with $k_0 = 6$ parameters: 2 coordinates, 2 proper motions, parallax and systemic RV. As a first approach, our simplest non-null hypothesis considers circular orbits, astrometric data only and one RV measurement. For a given period, the number of free parameters is then $k_P = 10$: the 6 kinematic ones plus the four Thiele Innes elements A, B, F and G (e.g. Wright & Howard 2009). Since the model is linear in all 10 parameters, the power can be efficiently computed for many periods between 20 days and 4000 days to obtain a familiar representation of the periodogram that we call a *Circular Least-squares Periodogram* (CLP). The CLP of the astrometric data, shown at top in Figure 1, displays two obvious peaks: the reported one at 270 days (Pravdo & Shaklan 2009) and a more significant one at 49.9 days, both with high power and very low FAPs.

To find the full Keplerian solution for both periods and estimate their FAPs, we perform a Least-squares periodogram sampling a grid of fixed eccentricity-period (eP) pairs and fitting all other parameters. For each eP pair k_P is 11: the null-hypothesis (X_0, Y_0, μ_X, μ_Y, π and v_0) plus all the other Keplerian elements: Mass of the planet, Ω, ω, i, and the Mean anomaly at the initial epoch M_0 (see Wright & Howard 2009, for a recent review). We analyze both *astrometry only* and *astrometry+RVs*. The χ^2 of the best fit solution is then used to obtain each FAP as previously described. Figure 1 shows the resulting color-coded FAPs for each eccentricity–period pair (eP-map).

3.1.1. Astrometry only

A value of $M = 300$ has been used to obtain the FAP, and our result at 270 d qualitatively agrees with Pravdo & Shaklan (2009), however the more significant period is at ∼50 d. For both periods, there are regions with FAP<1% spanning all possible eccentricities (second row in Figure 1). The best fits and their χ^2 per degree of freedom ($\bar{\chi}^2$) are summarized in Table 2. The obtained results for the 270 d period are in agreement with those reported in the discovery paper by Pravdo & Shaklan (2009). The best fit solution for the 50 d period has mass $\sim$ 15 M_J, which would be a very low mass brown dwarf. It is important to point out that the best fit inclination is close to 90 (edge on) for both solutions. The uncertainties on the orbital parameters are quantified in Sec 3.2.

3.1.2. Astrometry+RVs

We now fit jointly for the best orbital solution to the astrometry and RVs. Our campaign covered about 65% of the 270 d orbit. The standard deviation of all our RVs measurements is 250 m s^{-1} (null hypothesis) which is larger than the individual uncertainties in Table 4. When we cross-correlate our standards, we measure a similar RMS of 200 m s^{-1}, which indicates that the difference is due to an uncontrolled or unmeasured systematic. The RMS of the RVs for the best fit solution is 200 m s^{-1}, which is not statistically different from the RMS of the null hypothesis. This is another indication that our measurements contain systematic errors at the level of $100-200$ m/s. Despite of that, we use the nominal errors in the Least-squares solution as the best estimates for the individual uncertainties we can provide. In Figure 2, we show the best solutions to both signals including all the data.

For the 270 d period, our RV *non detection* cannot exclude a small region of orbital solutions around $e \sim 0.8$ with a FAP between 1%–5% – see Figure 1, third row right panel. We now add the RVs measurements by Z09 and solve for a joint solution. A zero-point offset between datasets is added as an additional free parameter. The combined RV measurements force the eccentricity to large values which apparently still provides a reasonable fit to the astrometry (see top panels in Figure 2). However, the FAPs are now all higher than 10% (Figure 1, bottom right panel), which indicates that the signal can be barely distinguished from the noise fluctuations. The "hint" of detection in Z09 based on one discrepant value at $3.1-\sigma$ out of five can be due to random errors with a non negligible probability.

For the 50 d period, there are still several orbits that provide a decent fit to the combined astrometry and the new RV data with a FAP lower than 1%. These occupy a small space around the best joint solution, with $e = 0.90$ (see Figure 1, 3rd row, left panel) and an inclination close to 0. Large eccentricity causes the duration of fast RV variation to be very short (and difficult to catch); an inclination close to 0 tends to suppress any RVs signal. Such inclination is in apparent contradiction with the one obtained using the astrometry alone ($\sim$ 90 deg). The reason is the following: while the new fit to the astrometry forced by the RVs is much worse than the one obtained from the astrometry alone, such a solution still represents an improvement compared to the null hypothesis. Adding Z09 data to the fit increases the FAP of the most likely solution to 2%, an eccentricity of 0.91 and the inclination close to 0 (see Table 2). This suggests that the signal at 50 d is also spurious, even though it has slightly better chances of survival than the one at 270 d.

3.2. *A Posteriori* Probability Distributions

We adapt the method developed by Ford (2005, 2006) to assess uncertainties in orbit determinations by obtaining the *a posteriori* probability distribution for the parameters using a Markov Chain with a Gibbs sampler strategy. Our problem is identical to the one described by Ford (2005), where now the χ^2 contains both RV and astrometric observations and the model has a few more

free parameters. Several properly adjusted MCMC with 10^6 steps have been computed obtaining compatible results. The step sizes of the Gibbs sampler are initialized with the formal errors from the best fit Least-squares solution, and adjusted to obtain a transition probability between 10% and 20%. The first 10^5 steps of each chain are rejected. The final distributions match very well the areas of low FAPs in the eP-maps (see Figure 3 as an example) giving further proof that the chains have converged to the equilibrium distributions. The MCMC contains 13 free parameters – the 11 from the Least-squares periodogram plus eccentricity and period. When the RVs measurements from Z09 are included, and additional offset parameter is included.

Table 2 presents the standard deviations obtained via the MCMC for both the 50 d and 270 d periods using astrometry alone and astrometry + all RV data. As an example, we show the two dimensional density of states in period-eccentricity space in Figure 3 (left) obtained in both cases around the 270 d signal. The marginalized distributions for e in the form of histograms are shown in Figure 3 (right). For the astrometry-alone case, the distribution of e is almost uniform. It becomes strongly peaked towards high eccentricities when all the RV data are included. Since the best fit solution at 270 d is poor ($\bar{\chi}^2 = 1.76$), the corresponding χ^2 minimum is not very deep which is reflected in a significant increase in the derived uncertainties (See Table 2). The same happens to the signal at 50 d with the exception of the inclination that has a small uncertainty (4 deg) close to 0. Even though this solution has a low FAP, the inclination has to be coincidentally very small to suppress any RV signal and very different from using astrometry only (94 deg), rasing serious doubts of its reality.

4. Discussion and Conclusions

The non-detection of a significant RV variation in our data set already discards most orbital configurations allowed by the astrometry. When combined with Z09 RVs measurements, there are no remaining solutions with a FAP lower than 10% around the 270 d period, so the presence of a planet candidate at that period is not supported by the observations. For the 50 d period, the constraints are also strong and become almost definitive when the Z09 data is included. Even highly eccentric solutions have a relatively large FAP ($> 2\%$). We find that particular combinations of eccentricity, inclination and ω can fit an almost flat RV curve indicating that the analytic methods applied to estimate FAPs for high eccentricities tend to give over optimistic results and that this issue should be studied in more detail.

We have developed and implemented useful tools for detailed analysis of combined astrometric and RV data: Circular Least-squares periodogram as the proper generalization of the classic Lomb-Scargle periodogram to deal with astrometric data, eP-maps to visualize the most likely period–eccentricity combinations and a Bayesian characterization of the parameter uncertainties based on a MCMC approach.

VB 10 is also part of the Carnegie Astrometric Planet Search program (Boss et al. 2009). RV

measurements with precision techniques in the near-infrared (Bean et al. 2009) may provide the required accuracy to put even stronger limits to the existence of VB10b or find other planets in the system. VB 10 will certainly be observed by the space astrometry mission Gaia (Perryman et al. 2001), which would be capable of finding a planet with a period of 270 d and as small as 0.2 M_J.

REFERENCES

Anglada-Escudé, G., Boss, A. P., & Weinberger, A. J. 2009, in ASP Conf. Ser., Vol. in press, Pathways Towards Habitable Planets, ed. V. Coudé du Foresto, D. M. Gelino & I. Ribas (San Francisco, CA: ASP)

Bean, J. L., Seifahrt, A., Hartman, H., Nilsson, H., Wiedemann, G., Reiners, A., Dreizler, S., & Henry, T. J. 2009, in ASP Conf. Ser., Vol. in press, Pathways Towards Habitable Planets, ed. V. Coudé du Foresto, D. M. Gelino & I. Ribas (San Francisco, CA: ASP), arXiv:0911.3148

Berger, E. et al. 2008, ApJ, 676, 1307

Black, D. C. & Scargle, J. D. 1982, ApJ, 263, 854

Bonfils, X. et al. 2007, A&A, 474, 293

Boss, A. P. et al. 2009, PASP, 121, 1218

Burgasser, A. J., Reid, I. N., Siegler, N., Close, L., Allen, P., Lowrance, P., & Gizis, J. 2007, in Protostars and Planets V, ed. B. Reipurth, D. Jewitt, & K. Keil (Tucson, AZ: Univ. of AZ Press), 427

Catanzarite, J., Shao, M., Tanner, A., Unwin, S., & Yu, J. 2006, PASP, 118, 1319

Cumming, A. 2004, MNRAS, 354, 1165

Cumming, A., Butler, R. P., Marcy, G. W., Vogt, S. S., Wright, J. T., & Fischer, D. A. 2008, PASP, 120, 531

Donati, J.-F., Jardine, M. M., Gregory, S. G., Petit, P., Bouvier, J., Dougados, C., Ménard, F., Cameron, A. C., Harries, T. J., Jeffers, S. V., & Paletou, F. 2007, MNRAS, 380, 1297

Donati, J.-F., Semel, M., Carter, B. D., Rees, D. E., & Collier Cameron, A. 1997, MNRAS, 291, 658

Fitzpatrick, M. J. 1993, in ASP Conf. Ser., Vol. 52, Astronomical Data Analysis Software and Systems II, ed. R. J. Hanisch, R. J. V. Brissenden, & J. Barnes, 472

Font-Ribera, A., Miralda Escudé, J., & Ribas, I. 2009, ApJ, 694, 183

Ford, E. B. 2005, AJ, 129, 1706

Ford, E. B. 2006, ApJ, 642, 505

Ford, E. B., Kozinsky, B., & Rasio, F. A. 2000, ApJ, 535, 385

Kelson, D. D. 2003, PASP, 115, 688

Nidever, D. L., Marcy, G. W., Butler, R. P., Fischer, D. A., & Vogt, S. S. 2002, ApJS, 141, 503

Perryman, M. A. C. et al. 2001, A&A, 369, 339

Pravdo, S. H. & Shaklan, S. B. 2009, ApJ, 700, 623

Scargle, J. D. 1982, ApJ, 263, 835

Scholz, A., Jayawardhana, R., , & Wood, K. 2006, ApJ, 645, 1498

Tamuz, O. et al. 2008, A&A, 480, L33

van Biesbroeck, G. 1961, AJ, 66, 528

Vogt, S. S. et al. 1994, in SPIE Conf. Ser., Vol. 2198, Instrumentation in Astronomy VIII, ed. D. L. Crawford & E. R. Craine, 362

Wright, J. T. & Howard, A. W. 2009, ApJS, 182, 205

Zapatero-Osorio, M. R., Martín, E. L., del Burgo, C., Deshpande, R., Rodler, F., & Montgomery, M. M. 2009, A&A, 505, L5

Table 1. Log of RVs

Telescope +Instrument	UT Date	HJD –2450000	Slit Width $''$	RV (w/ GJ 699)[a] km s^{-1}	RV (w/ GJ 908)[a] km s^{-1}
Keck I + HIRES	2006 Aug 12	3959.57	0.86	–	35.59 ± 0.15
Clay+MIKE	2009 Jun 06	4988.74	0.35	36.23 ± 0.13	35.99 ± 0.15
Clay+MIKE	2009 Jun 07	4989.82	0.50	36.22 ± 0.13	36.09 ± 0.20
Clay+MIKE	2009 Jun 08	4990.75	0.50	36.15 ± 0.12	36.10 ± 0.22
Clay+MIKE	2009 Jun 30	5012.72	0.35	35.72 ± 0.11	–
Clay+MIKE	2009 Jul 25	5037.66	0.50	35.96 ± 0.11	36.03 ± 0.11
Clay+MIKE	2009 Sep 04	5078.58	0.50	35.96 ± 0.09	36.37 ± 0.24
Clay+MIKE	2009 Oct 15	5119.54	0.50	36.30 ± 0.14	36.41 ± 0.13
Clay+MIKE	2009 Oct 26	5130.51	0.50	36.41 ± 0.16	36.27 ± 0.18
CFHT+ESPaDOnS	2009 Nov 29	5164.69	–[b]	–	35.74 ± 0.20

[a]Uncertainties are the standard deviation of the 9 orders of the cross correlation and do not include the 40 m s^{-1} systematic uncertainty from the telluric wavelength correction. Absolute radial velocity determination has an uncertainty of 0.4 km/s but it is not relevant for orbital fitting purposes.

[b]ESPaDOnS is a fiber fed spectrograph with an effective resolution of R∼68000 in the wavelength range of interest

Table 2. Best fitting values[a] . Uncertainties obtained from a MCMC with 10^6 steps.

Parameter	Astrometry 50 d	Astrometry 270 d	Astro+ all RV 50 d	Astro+ all RV 270 d
X_0(mas)	-16.6 ± 1.6	-14.1[d] ± 3.2	-21.15 ± 2.3	-17.9 ± 4.7
Y_0(mas)	-408.0 ± 1.9	-406.1[d] ± 3.5	409.52 ± 2.8	-410.5 ± 5.51
$\mu_{\rm R.A.}$(mas/yr)	-588.98± 0.25	-589.08 ± 0.25	-588.66 ± 0.29	-589.21 ± 0.26
$\mu_{\rm Dec}$(mas/yr)	-1360.95± 0.25	-1361.08 ± 0.24	-1361.02 ± 0.25	-1361.36 ± 0.20
π(mas)	168.3 ± 1.51	169.5 ± 1.4	169.95 ± 1.37	169.24 ± 1.30
v_0(km/s)	35.2 ± 1.4	35.4[d] ± 1.050	36.06 ± 0.11	36.05 ± 0.08
$v_{\rm offset}$(km/s)	-	-	1.5 ± 0.42	1.5 ± 0.36
P(days)	49.7 ± 0.5	272.1 ± 4.1	49.84 ± 0.11	278.5 ± 2.7
$Mass$(M$_{\rm J}$)	17.5 ± 4.4	7.1 ± 2.7	13.7 ± 6.4	5.0 ± 2.9
e	0.22[c] ± 0.30	0.48[c] ± 0.31	0.91 ± 0.13	0.90 ± 0.16
i(deg)	93 ± 5	90 ± 15	4 ± 5	110[c] ± 50
Ω(deg)	40 ± 20	220 ± 25	13[c] ± 100	40[c] ± 66
ω(deg)	20 ± 40	30[c] ± 80	122[c] ± 60	17[c] ± 90
M_0(deg)	270 ± 0	170[c] ± 108	340[c] ± 70	156[c] ± 80
a(AU)[d]	0.12	0.36	0.12	0.36
$\bar{\chi}^2_0$	2.28	2.28	2.75	2.75
$\bar{\chi}^2$	0.87	0.93	1.62	1.76

[a]The mass of VB 10 is assumed to be 0.078 M$_\odot$ according to Pravdo & Shaklan (2009)

[b] Large uncertainty due to correlation with the eccentricity

[c]Unconstrained or poorly constrained

[d]Derived quantity using Kepler equations

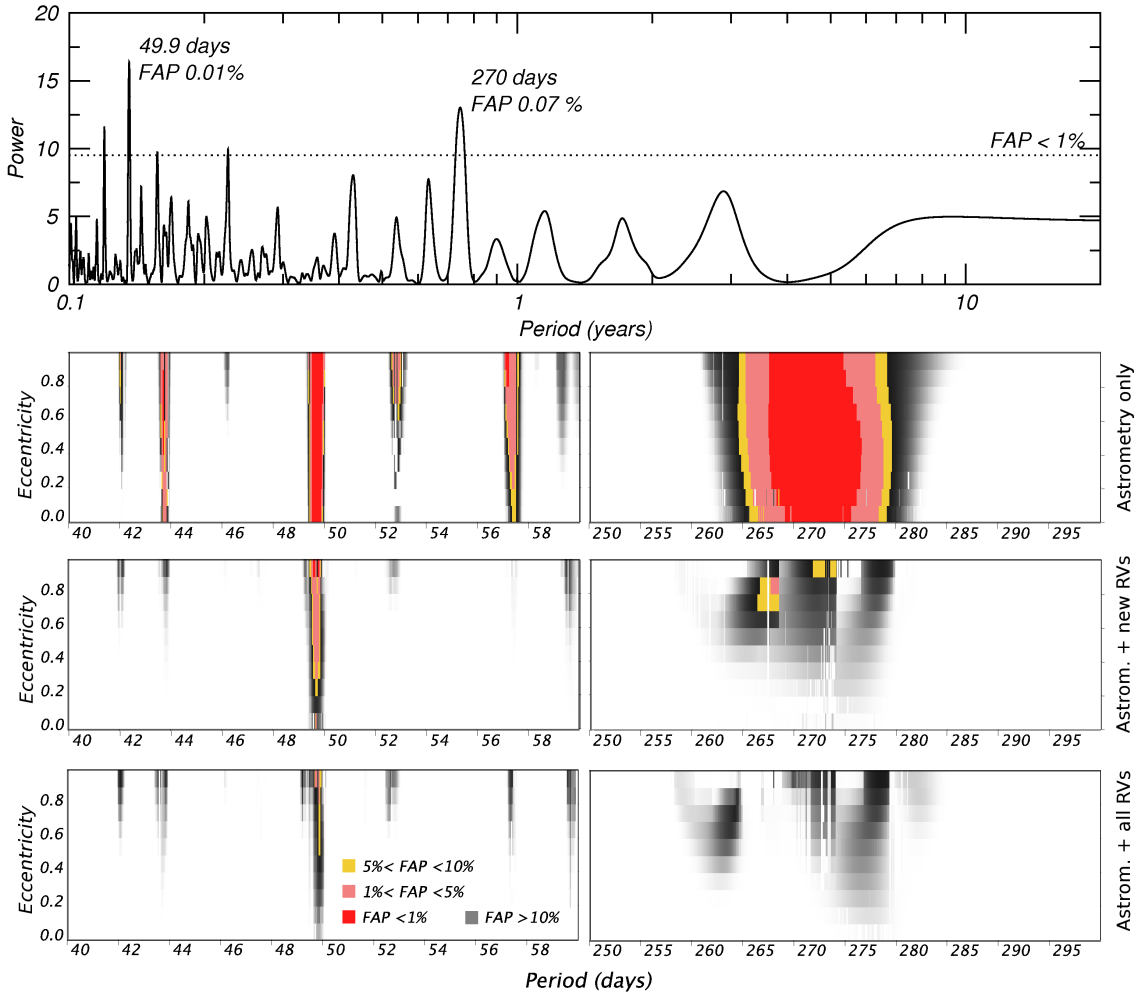

Fig. 1.— **Top panel.** Circular Least-squares periodogram showing the two most significant periods with their corresponding False Alarm Probabilities (FAP). **Second row.** FAPs obtained for a grid of Eccentricity–Period pairs around the 50 d (left) and the 270 d (right) when only astrometry is considered. **Third row.** FAPs obtained when our new RV are included to the fit. **Bottom row.** Final FAPs obtained when all published RV data are combined in a joint fit.

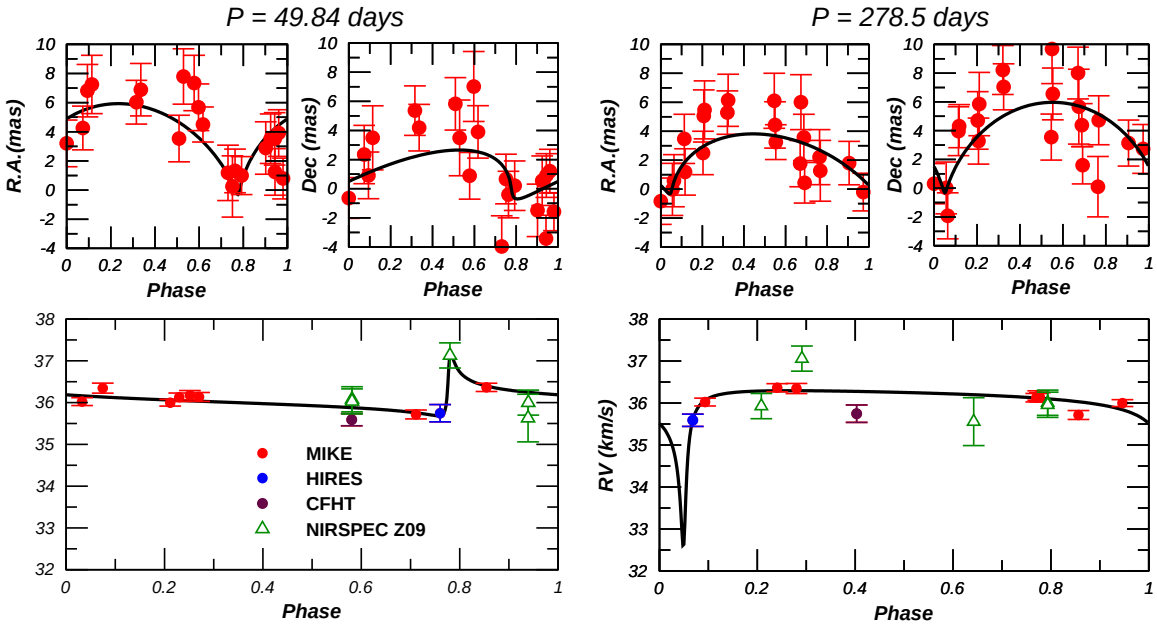

Fig. 2.— The best fit (lowest χ^2) joint solutions to the Pravdo & Shaklan (2009) astrometry and used RVs for the two signals. Top panels contain the astrometric offsets after the removal of the corresponding parallax and the proper motion. The lower panels contain all RVs used. Each RV point represents the weighted average of the values obtained using both reference stars if available. The best fit offset has been applied to Z09 data (Green triangles). Phase 0 corresponds to the first astrometric epoch at JD 2451438.64 and the corresponding folding periods are given on the top.

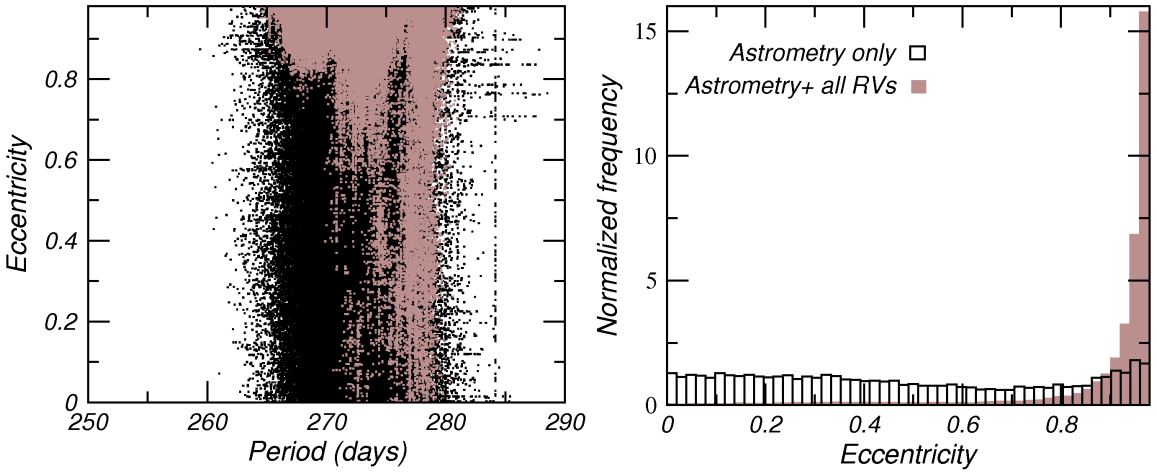

Fig. 3.— Left: Steps in period-eccentricity space of a Markov Chain of 10^6 elements applied to the astrometry only (black) and to the astrometry+all RV data (brown). The distribution resembles the FAP contours on the eP-maps around 270 days indicating that the chain has successfully converged to the equilibrium distribution. Right: Histogram reproducing the marginalized density distributions in e for the astrometry only and astrometry+RV around the 270 d solution.